ANALYSIS AND DESIGN OF COPLANAR WAVEGUIDE FOR HIGH-SPEED PULSE PROPAGATION ON PRINTED CIRCUIT BOARD

MOHD MUHAIYIDDIN BIN ABDULLAH

UNIVERSITI SAINS MALAYSIA

2007

ANALYSIS AND DESIGN OF COPLANAR WAVEGUIDE FOR HIGH-SPEED PULSE PROPAGATION ON PRINTED CIRCUIT BOARD

by

MOHD MUHAIYIDDIN BIN ABDULLAH

Thesis submitted in fulfillment of the requirements for the degree of Master of Science

September 2007

ACKNOWLEDGEMENTS

Alhamdulillahi Rahman Ir Rahim.

First and foremost, I would like to express my sincere gratitude and acknowledgement to Professor Syed Idris Bin Syed Hassan for all the guidance and feedback throughout the course of this research. I also would like to thanks USM board of reviewers and Dr. Widad Binti Ismail for their comments and constructive feedback on the contents and organization of this thesis. I also would like to show my appreciation to staffs of School of Electrical and Electronic Engineering, University Sains Malaysia (administration, library and laboratory) for their supports in various capacities during these years.

I also would like to express my sincere appreciation to my employer, Intel Malaysia and all my managers for providing supports, encouragements and more importantly the environments for the success of this research.

I would like to dedicate this work to my family; my beloved wife Aida, and my children Jazmin, Wardina and Dahlia for their continuous encouragements and for giving me time to finish this thesis. Lastly, I would like to express my heartfelt appreciations to my parents for inculcating the importance of long life learning in me.

TABLE OF CONTENTS

LIST OF TABLES

LIST OF FIGURES

LIST OF SYMBOLS

		Page
h	Dielectric thickness	2
ε_r	Dielectric constants	4
tanδ	PCB dissipation factor or loss tangent	4
ε_{eff}	Effective dielectric constant	6
Z_o	Characteristic impedance	6
L	Inductance (Henry)	8
C	Capacitance (Farad)	8

V	Voltage (Volt)	8
I	Current (Ampere)	8
z	Location or distance from the origin (meter)	9
t	Time (second)	9
R	Resistance (Ohm, Ω)	10
G	Conductance (Siemens)	10
α	Attenuation constant	11
β	Phase constant	11
γ	Propagation constant	11
λ_g	Guided wavelength (meter)	12
c	Speed of light in vacuum (approximately 3.0×10^8 m/s).	12
J_o	Current density (A/m^2)	13
ρ	Resistivity (Ω/m)	13
R_{dc}	DC resistance	13
R_{ac}	High frequency resistance	13
R_s	Surface resistance	13
δ	Skin depth	14
μ	Material permeability (H/m)	14
σ	Conductivity (S/m)	14
A_{eff}	The frequency dependent effective cross-section area	15
I_o	The current magnitude	16
w	Trace width	16
f	Frequency (Hertz)	24
τ	The pulse width at the middle crossing points of maximum and minimum amplitude	28
V_o	Voltage amplitude	28
E	Electric Field	34
B	Magnetic field	34
C_o	Capacitance using vacuum as the dielectric material	37
ϕ	Elliptical integral phase	38
w_g	Top strip width	39
b-a	Air gap of the CPW	39
q	The filling factor of the structure	41
f_{knee}	Knee frequency	48
T_r	Rise time	48
f_o	fundamental frequency	50

R^2_E	Statistical squared error	51
l_g	Transmission line length	67

LIST OF ABBREVIATION

		Page
FR4	Flame Resistant 4, a type of material commonly used on PCB	2
MMIC	Monolithic microwave integrated circuit	3
PCB	Printed circuit board	3
CPW	Co-planar waveguide	3
i.e.	That is	3
TEM	Transverse electric and magnetic	5
QS-TEM	Quasi-static TEM	5
EM	Electromagnetic	8
p.u.l.	Per-unit length	8
m	Meter	8
S/m	Siemens per meter	11
Hz	Hertz	14
MS	Microstrip	17
SL	Slot line	19
CPS	Coplanar stripline	19
MEMS	Micro-electromechanical systems	20
CB-CPW	Conductor-backed CPW	21
3D	Three dimensions	25
H-field	magnetic field	25
E-field	Electric field	25
FWHM	A full width of half maximum	28
SDA	Spectral domain analysis method	34
CM	Conformal Mapping	35
V_{ph}	Phase velocity	37
GaAs	gallium arsenide	39
mm	Millimeter (i.e. 1/1000 of a meter)	40
RMS	Root-mean squared	51
TE	Transverse Electric	52
f_{TE}	Cut-off frequency for the lowest order transverse electric	52
PPM	Parallel plate mode	55

SCPW	Suspended CPW	55
RF	Radio frequency	57
MW	Microwave	57

LIST OF APPENDICES

LIST OF PUBLICATIONS & SEMINARS

1. Abdullah, M. M. and Syed Idris, S. H., Analysis and Design of Coplanar Waveguide for High-Speed Pulse Propagation on Printed Circuit Board, USM EE Academic Seminar, 27 February 2007.

ANALISA DAN REKABENTUK PANDU GELOMBANG SESATAH UNTUK PERAMBATAN DEDENYUT BERKELAJUAN TINGGI DI ATAS PAPAN LITAR.

ABSTRAK

Tujuan tesis ini adalah untuk menyelidik struktur pandu gelombang sesatah (CPW) yang sesuai bagi kegunaan papan litar (PCB) untuk perambatan dedenyut berkelajuan tinggi, untuk menjalankan kajian menyeluruh mengenai ciri-ciri perambatan dan juga untuk membandingkan keupayaan dengan talian mikrostrip. Rumus-rumus rekabentuk telah dibangunkan berdasarkan rumus-rumus yang asalnya disyorkan kepada MMIC dan silikon CPW. Kemudiannya, rumus-rumus ini telah digunakan untuk mengoptimumkan rekabentuk CPW dimana keputusan-keputusannya menunjukkan perbezaan sebanyak 15% dibandingkan dengan keputusan-keputusan simulasi. Analisa-analisa domain frekuensi dan domain waktu telah dijalankan secara menyeluruh untuk mengenal pasti kesan parameter-parameter CPW ke atas keupayaan perambatan dedenyut. Selepas itu, satu litar prototaip telah dibangunkan untuk mengesahkan keputusan-keputusan teori dan simulasi. Ukuran bacaan eksperimen menunjukkan persamaan yang ketara dengan keputusan-keputusan teori dan simulasi disamping mengetengahkan beberapa isu lain. Berlawanan dengan pendapat popular yang mengatakan CPW lebih berkeupayaan dari talian mikrostrip berdasarkan pengalaman MMIC, tesis ini menunjukkan berbagai isu-isu bagi aplikasi CPW di atas papan litar seperti kejadian salunan (resonance) mendatar dan menegak yang kuat. Menariknya, isu-isu ini tidak dikesan di dalam mana-mana simulasi mengunakan model ADS ataupun dari rumus-rumus rekabentuk. Lalu, tesis ini telah berjaya mengesyorkan pendekatan-pendekatan alternatif untuk simulasi ADS dan rumus-rumus bagi memberi ramalan yang lebih realistik kepada ciri-ciri litar yang sebenar. Terakhirnya, beberapa topik kajian berkenaan dengan papan litar CPW telah disyorkan untuk kajian mendalam bagi menjadikan struktur CPW lebih popular untuk kegunaan dedenyut berkelajuan tinggi di atas papan litar.

ANALYSIS AND DESIGN OF COPLANAR WAVEGUIDE FOR HIGH-SPEED PULSE PROPAGATION ON PRINTED CIRCUIT BOARD

ABSTRACT

The goals of this thesis are to investigate a suitable printed circuit board (PCB) coplanar waveguide (CPW) for high-speed signal propagation application, to conduct thorough analyses of its propagation characteristic and to compare its performance against the mainstream microstrip line. Design equations are developed by adopting expressions that are originally proposed for monolithic microwave integrated circuit (MMIC) and silicon CPW. Then, these equations are employed for optimized CPW designs whereby the results are compared to simulations outputs for sanity checks that showed 15% differences. Extensive frequency and time domain numerical analyses are conducted to access the impacts of each CPW parameters to signal propagation performance. Subsequently, a prototype circuit is built to verify theoretical and simulations results. Experiment results show excellence correlations to theoretical estimates as well as exposed some potential issues. Contrary to popular beliefs that CPW has superior performance than microstrip based on MMIC experience, this thesis unveiled various CPW issues for larger scale PCB implementation such as severe lateral and longitudinal resonances. Interestingly, these issues are not detected by ADS simulations using the built-in CB-CPW model or by the design equations. Thus, the thesis has successfully proposed alternatives approaches for ADS simulations and design equations for more realistic predictions of the actual circuit characteristics. Lastly, a few potential research topics on PCB CPW structures were highlighted for further researches for making CPW to be more compelling for high-speed PCB implementations.

CHAPTER 1

INTRODUCTION

1.0 Background

Chip level frequency is increasing rapidly following a remarkable progress in semiconductor processes and on-chip interconnects technologies (ITRS, 2005). However, clearly from Figure 1.1, the off-chip frequency is lagging due to various issues related to off-chip interconnects. One of the issues is contributed by transmission line effects that are getting more prevalent at higher frequency as the circuit length comparable to the signal wavelength.

Figure 1.2 illustrates a simplified high-speed link consisting of a transmitter, transmission mediums and a receiver. In general, these transmission mediums need to provide adequate bandwidth to ensure negligible distortions to the propagating high-speed signals. Some examples of transmission line mediums are on-chip interconnects, package interconnects, socket, via, transmission line and cables. Typical issues associate with off-chip interconnects are originated in transitional vias, sockets and transmission lines. For the former two, radiation and crosstalk are the main issues originated from impedance discontinuities and crosstalk. Via impedance mismatch can be solved by using stub-less via to avoid opened circuit quarter wavelength resonance, micro-via or control impedance via (Antonini et al., 2004; Pillai, 1997). Similar approaches have been taken to avoid crosstalk and radiation of the

socket by venturing into control impedance socket and shielded pin (Ortega and Elco, 1999).

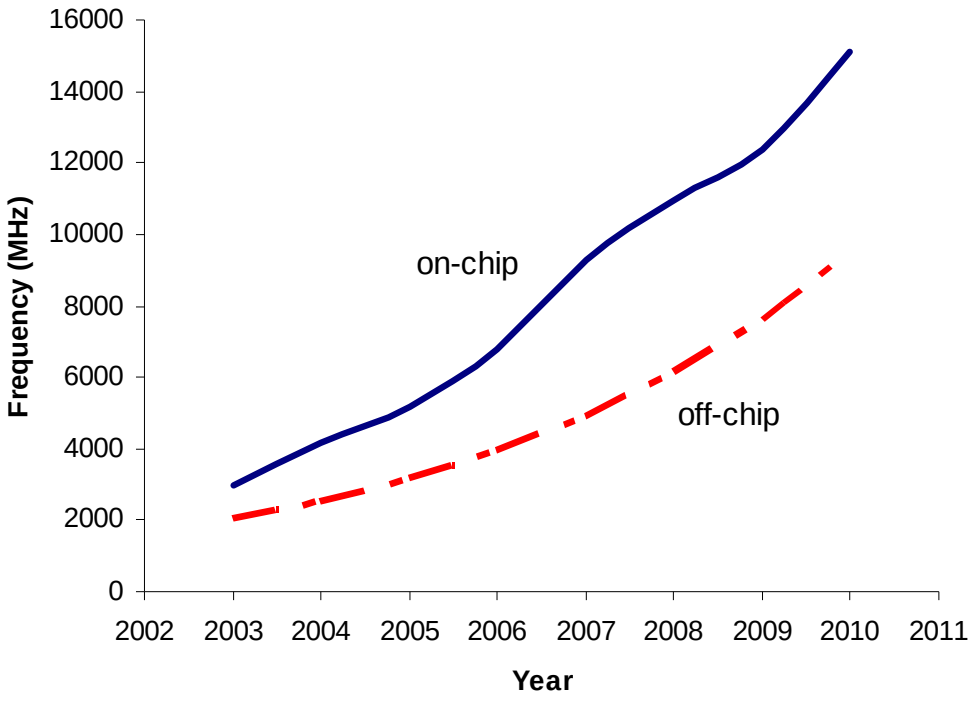

Figure 1.1: A near term trend for on-chip wiring frequency (ITRS, 2005)

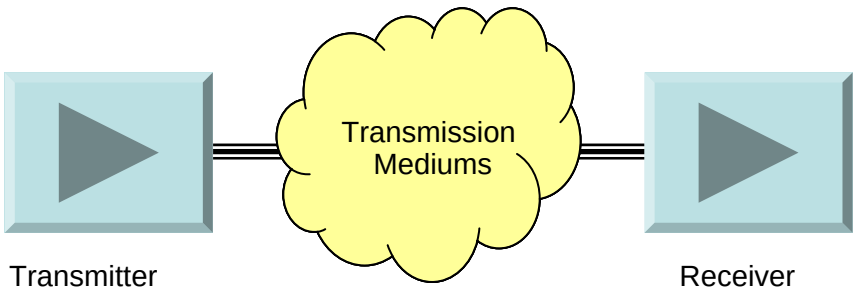

Figure 1.2: A signal transmission block diagram showing the key components: a transmitter, transmission mediums, and a receiver.

There are many transmission lines available to meet various applications. The most popular ones are strip and microstrip lines as shown in Figure 1.3. Typically, the conductors are made of copper and the dielectric materials are based on FR4 dielectric material. Strip and microstrip transmission lines perform well at lower and medium frequency range; but may post concerns at high-frequency region. Reflections and

radiations losses are the main issues for strip and microstrip lines that are induced by connecting vias. In addition, microstrip line presents additional challenges to high-speed pulse propagation in term of crosstalk susceptibility, radiation emissions and signal dispersions. Crosstalk and radiation are largely caused by poor shielding while dispersion is created by inhomogeneous dielectric material interfaces.

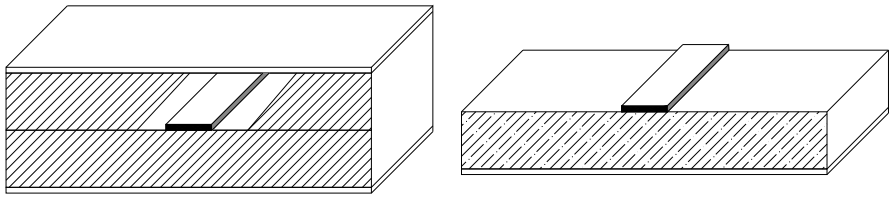

(a) (b)

Figure 1.3: Two most common PCB transmission lines: (a) Stripline and (b) microstrip transmission lines.

Another popular transmission line is coplanar waveguide (CPW) which is generally assumed performing better than stripline or microstrip. This advantage is mainly attributed to the absent of connecting via, good access to grounding points and lower dispersion characteristics (Simon, 2001). The applications of CPW for high frequency MMIC applications has been widely researched and reported in numerous literatures (Simon, 2001). However, limited researches are being done for CPW implementation on larger printed circuit board (PCB) circuits except for a noticeable few such as from El-Badawy and El-Sharawy (1992) and Bokhari and Ali (2003). This awareness inspires the author to embark on this research topic to investigate the CPW signal propagation behavior in details and it prospect for high-speed data transmissions on PCB. Some of the main concerns related to direct proliferations of MMIC CPW design rules to PCB design are listed for further investigations:

i) Physical Differences

A 50-Ω FR4 PCB CPW requires a ratio of dielectric height to trace width of about the same dimension (i.e. unity). On the other hand, 50-Ω MMIC CPW requires

dielectric to trace width ratio of 2 to 7 times larger (Shih, 1991). Therefore, significant electrical behaviors differences are expected especially on dispersions and parallel plate resonance frequencies. In general, PCB channels are longer than MMIC channels by 25mm (1 inch) to 150mm (6 inches) or more. Apparently, PCB trace lengths are a lot bigger than one-half of the maximum wavelength of interest, (i.e. $>\lambda/2$). Thus, the transmission line effects are expected to be more prominent on PCB compared to MMIC.

ii) Propagation Medium Differences

PCB material dielectric constants (ε_r) are within 3.0 to 4.0, while MMIC has higher ε_r of 10 to 15. As a consequence, different propagation characteristic and physical dimensions (trace width, and air gap) are expected to give direct impact to propagating signals performance in terms of dispersions and attenuations.

iii) Attenuation Differences

PCB dissipation factor or loss tangent ($\tan\delta$) is higher attributed to bigger dissipation factors of 0.005 to 0.023 compared to GaAs of only 0.001 (very low loss). Loss tangent (dielectric polarization and imperfections) contributed to the dielectric material losses in addition to the conductor losses. This is particularly important for PCB attributed to its larger circuit dimensions that make dielectric loss significant. Furthermore, dielectric loss tangent are more dominant on PCB compared to conductor losses at higher frequency (Johnson and Graham, 2004).

Thus, these differences warrant thorough analyses for the PCB CB-CPW transmission line behavior analyses to ensure performance and stability across the intended frequency range.

1.1 Thesis Objectives

The objectives of this thesis are:

i) To investigate a suitable CPW structure for high-speed pulse propagation.

ii) To study the CPW propagation behaviors through numerical analysis, simulations and measurements.

iii) To compare CPW propagation characteristics and overall performance to microstrip transmission line.

The main contributions out of this thesis are:

i) To present validated transmission line equations for attenuation and propagation constant of the chosen CPW variant that is fully backed to correlate to simulation and measurement data.

ii) To propose design rules for the applications of the chosen CPW for PCB high-speed pulse propagation.

1.2 Thesis Scope of Work

Since it is impossible to comprise all elements related to the subject under study, therefore, this work will focus within the following boundaries. Firstly, mathematical equations and solutions for standard transmission line equations will be omitted for brevity with references are given in the bibliography for interested readers. Similarly, mathematical problems are solved using look-up tables or computer programs without showing the derivation details.

Secondly, commercial software tools will be used for analytical and numerical calculations as well as for structures modeling. MATLAB® version 7 will be employed for numerical calculations and Agilent's Advanced Design System (ADS) for all linear circuit simulations using modeled and measured data. Ansoft Corporation's 2D Extractor™ electromagnetic (EM) modeling software will be utilized for quasi-

transverse electric and magnetic (QS-TEM) analysis and High Frequency Structure Simulation (HFSS™) for full-wave modeling. The genuine intention to minimally employ these simulations tools for checking the calculated values. For information, there are other equivalent software packages available for each of the tools other than those mentioned above. For example, Quasi-TEM field solver and full-wave field solver alternatives are also available from CST (www.cst.com) and Agilent (www.agilent.com). As for numerical analysis, there are many alternatives available including some free tools from the internet.

Thirdly, the operating frequency is limited up to 40GHz to facilitate the measuring equipment bandwidths and numerical analysis QS-TEM assumption limits. Finally, the study will be limited to a typical PCB configuration in term of material properties and physical dimensions.

1.3 Thesis Organization

This dissertation is divided into eight chapters. Chapter 1 covers the introduction, project objectives, scopes of work and overall thesis organization. Chapter 2 reviews general transmission line theories, planar transmission line structures and literature survey associated to CPW analysis and analyses methodologies to pave the way for subsequent discussions in future chapters. Chapter 3 reviews the methodologies to be employed for frequency domain, time domain analyses as well as measurement setup. Chapter 4 illustrates the approaches for deriving CB-CPW QS-TEM relations to characteristic impedance (Z_o) and effective dielectric constant (ε_{eff}).

Next, Chapter 5 enhances the QS-TEM formulations from Chapter 4 by incorporating the frequency dependent effects. Then, the derived frequency dependent QS-TEM based equations will be validated against data from literatures and full-wave

simulation. Then, analyses on key parameters of the CPW will be performed to evaluate their influence to the overall circuit performance for design optimizations purposes.

Subsequently, Chapter 6 focuses to review frequency and time domain analyses results to measure the overall performance in both worlds. Frequency domain analyses are useful to give the overall design preview highlighting design optimization opportunities, whereas, equally important time domain (transient) analyses give performance indicator against amplitude and timing specifications in which digital systems are typically based upon. Then, Chapter 7 is devoted to review measurement results of the prototype CB-CPW circuits and how well they correlate to the results from the developed CB-CPW design equations.

Lastly, Chapter 8 summarizes the projects accomplishments against the set objectives and expected contributions. Chapter 8 also outlines some related topics for future explorations.

CHAPTER 2

REVIEW OF TRANSMISISON LINE THEORY

2.0 Introduction

Transmission line study is one of the electrical engineering foundations that are covered in many engineering text books such as Field and Wave Electromagnetic (Cheng, 1989), Fields and Waves in Communication Electronics (Ramo et al., 1993), and Fields Theory of Guided Waves (Collin, 1993). Cheng and Ramo's describe the relationships between plane electromagnetic (EM) waves to the general circuit theory. Collin's explains ample transmission line equation derivations and thorough explanations of their relation to EM theories. The main goal of this chapter is to give a brief overview of transmission line theory to facilitate future discussions on transmission line equations in later chapters.

2.1 Ideal Transmission Line

A general ideal transmission line model with microscopic length dz is shown in Figure 2.1. Whereby, L is the inductance per-unit length (p.u.l) (Henry/meter) and C is the capacitance p.u.l (Farad/meter). Voltage (V) and current (I) p.u.l. are given by Equation 2.1 and Equation 2.2 famously known as telegraphers' equations (Ramo et al, 1993):

$$\frac{\partial V}{\partial z} = -L\frac{\partial I}{\partial t} \tag{2.1}$$

$$\frac{\partial I}{\partial z} = -C\frac{\partial V}{\partial t} \qquad (2.2)$$

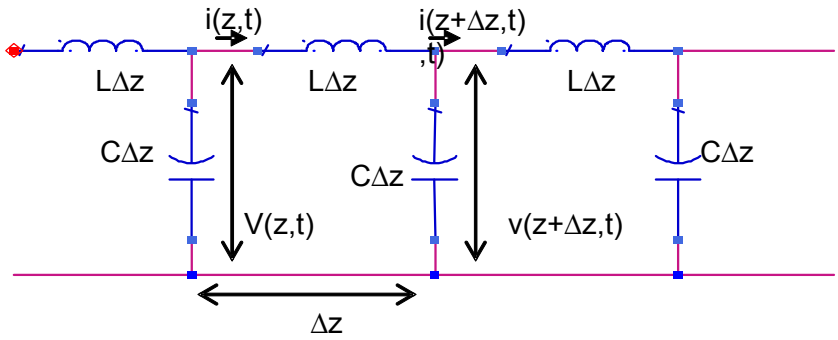

Figure 2.1: An infinitesimal representation of a general ideal transmission line segment. (t=time, z=distance, v=volt and i=current).

Next, Table 2.1 summarizes the transmission line equations and their relations to the Maxwell's plane wave equations (Ramo et al., 1993).

Table 2.1: Comparisons between Transmission Line Equations and Plane Wave Equations.

Operation	Transmission Line Equations (in term of Voltage and Current)	Maxwell's plane wave Equations (in term of *E* and *H* Fields)
Differentiate with respect to *z*	$\frac{\partial^2 V}{\partial z^2} = -L\frac{\partial^2 I}{\partial z \partial t}$ (2.3)	$\frac{\partial^2 Ex}{\partial z^2} = -\mu\frac{\partial^2 Hy}{\partial z \partial t}$ (2.4)
Differentiate with respect to *t*	$\frac{\partial^2 I}{\partial t \partial z} = -C\frac{\partial^2 V}{\partial t^2}$ (2.5)	$-\frac{\partial^2 Hy}{\partial t \partial z} = -\varepsilon\frac{\partial^2 Ex}{\partial t^2}$ (2.6)
Substitution	$\frac{\partial^2 V}{\partial z^2} = LC\frac{\partial^2 V}{\partial t^2}$, since $v = \frac{1}{\sqrt{LC}}$, where v is velocity $\Rightarrow \frac{\partial^2 V}{\partial z^2} = \frac{1}{v^2}\frac{\partial^2 V}{\partial t^2}$ (2.7) similarly $\Rightarrow \frac{\partial^2 I}{\partial z^2} = \frac{1}{v^2}\frac{\partial^2 I}{\partial t^2}$ (2.8)	$\frac{\partial^2 Ex}{\partial z^2} = -\mu\varepsilon\frac{\partial^2 Ex}{\partial t^2}$, since $v = \frac{1}{\sqrt{\mu\varepsilon}}$ $\Rightarrow \frac{\partial^2 Ex}{\partial z^2} = \frac{1}{v^2}\frac{\partial^2 Ex}{\partial t^2}$ (2.9) similarly $\Rightarrow \frac{\partial^2 Hy}{\partial z^2} = \frac{1}{v^2}\frac{\partial^2 Hy}{\partial t^2}$ (2.10)

All functions inside Table 2.1 are assumed continuous so that they can be substituted into each other to yield one dimensional wave equations (in z direction for Equations 2.3 to Equation 2.10).

Equation 2.8 has a general solution in this form (Ramo et al., 1993):

$$I = \frac{1}{Z_0}\left\{F_1(t-\frac{z}{v}) - F_2(t+\frac{z}{v})\right\} \tag{2.11}$$

Where, F_1 and F_2 are arbitrary functions and Z_o is defined below.

$$Z_0 = Lv = L\frac{1}{\sqrt{LC}} = \sqrt{\frac{L.L}{LC}} = \sqrt{\frac{L}{C}} \quad \text{(ohm)} \tag{2.12}$$

The derived constant Z_0 is known as characteristic impedance. Z_0 is defined as the ratio of voltage to current for any traveling waves at any given points (z) and at any given instances (t).

2.2 Non-Ideal Transmission Line

In reality, transmission lines are non-ideal attributed to various losses that present in many forms. In general, a non-ideal transmission line can be modeled as shown in Figure 2.2 below with two additional elements—resistance (R) and conductance (G). These additional terms can be viewed as corrections for the lateral ohmic losses (R) and vertical material leakages losses (G) respectively.

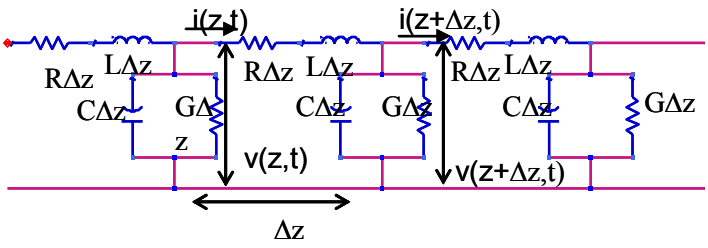

Figure 2.2: An infinitesimal representation of a general non-ideal transmission line segment.

Where, R is the resistance p.u.l (Ohm/meter), L is the inductance p.u.l (Henry/meter), C is the capacitance p.u.l (Farad/meter) and G is conductance p.u.l (Siemens/meter). Next, a non-ideal line characteristic impedance (Z_o) is given by:

$$Z_0 = \frac{Z}{\gamma} = \sqrt{\frac{Z}{Y}} = \sqrt{\frac{(R + j\omega L)}{(G + j\omega C)}} \quad \text{(ohm)} \tag{2.13}$$

Apparently, Equation 2.13 suggests that for a non-ideal transmission line case, characteristic impedance (Z_0) is a complex entity implying that traveling wave's voltages and currents are not necessarily in phase. When R and G terms are forced to zero as in loss-less case, Equation 2.13 reduced to the same form as Equation 2.12. Equation 2.13 also introduced a new term γ ("gamma") which represent another important transmission line parameter known as propagation constant. A complete γ expression is shown below (Ramo et al., 1993):

$$\gamma = \alpha + j\beta = \sqrt{ZY} \tag{2.14}$$

Next, substituting Equation 2.11 into Equation 2.13 will yield Equation 2.15, where α ("alpha") signifies the rate of exponential attenuation p.u.l. or commonly known as attenuation constant (in Neper/meter), while β ("beta") represents the amount of phase shift per-unit length for each wave or commonly referred as phase constant (in radian/meter).

$$V = V_+ e^{-\alpha z} e^{-j\beta z} + V_- e^{+\alpha z} e^{+j\beta z} \ \textbf{(V)} \tag{2.15}$$

A total attenuation constant (α) for a general transmission line is given by Equation 2.16 (Haydl, 1997):

$$\alpha = \alpha_c + \alpha_d + \alpha_r + \alpha_{\mathrm{mod}\,e} + \alpha_{cond\_sub} \text{ (Neper/m)} \qquad (2.16)$$

where α_c, α_d, α_r, α_{mode}, α_{cond_sub} are attenuation constants for conductor, dielectric material polarization (dielectric loss), radiation, modes conversion, and non-zero substrate conductivity respectively.

Next, the phase constant (β) is defined by Equation 2.17 below (Ramo et al., 1993):

$$\beta = \frac{2.\pi}{\lambda_g} = \frac{2.\pi.f\sqrt{\varepsilon_{eff}}}{c} \quad \text{(radian/m)} \qquad (2.17)$$

where, λ_g is the guided wavelength in meter (m), f is the frequency in Hertz (Hz), and c is the speed of light in vacuum (approximately 3.0×10^8 m/s). General expressions for α and β are summarized in table 2.2 below for all the three cases: non-ideal, ideal and low-loss line transmission lines (Ramo et al., 1993).

Table 2.2: General α and β expressions for General Transmission Line, Ideal Line, and Low Loss Line (from Ramo et al. page 249)

Quantity	Non-ideal line	Ideal Line	Approximation for Low-loss Line
α	Real $\{\sqrt{(R+j\omega L)(G+j\omega C)}\}$	0	$\frac{R}{2Z_0}+\frac{GZ_0}{2}$
β	Imaginary $\{\sqrt{(R+j\omega L)(G+j\omega C)}\}$	$\sqrt{\frac{L}{C}}$	$\sqrt{\frac{L}{C}}\left[1+j\left(\frac{G}{2\omega C}-\frac{R}{2\omega L}\right)\right]$

2.3 DC and Frequency Dependent Resistance

Low frequency and high frequency currents behave differently inside the conductor. This section explains the differences between low and high currents distributions in detail though theoretical analyses and field solver simulations.

2.3.1 DC and Low Frequency Resistance

Low frequency current density (J_o, A/m^2) is evenly distributed inside the conductor. Therefore, low frequency resistance p.u.l. formula is similar to that of the standard DC resistance as shown by Equation 2.18 below:

$$R_{dc} = \frac{\rho}{A} \qquad (\Omega/\text{meter}) \qquad (2.18)$$

where, ρ is the resistivity of the conductor (unit in ohm/m) and *A* is the cross sectional area of the line (unit in m^2).

2.3.2 High Frequency Resistance

High frequency resistance (R_{ac}) is difficult to estimate because of the complexity to determine the frequency dependent depth of penetration or commonly known as skin effect. Classical skin effect approximation was developed by Wheeler (1942) in his paper "Formulas for the Skin-Effect." Wheeler expression was developed based on surface resistance (R_s) related to the incremental inductance associated with penetration of magnetic flux into the conductor surface (Denlinger,1980). Over the years, various authors have refined Wheeler's estimations through synthesis methods, curve fittings and laboratory experiments (Waldow and Wolff, 1985; Pucel, 1968).

Theoretically, low-frequency currents tend to flow following least resistance paths, whereas high frequency currents tend to follow least inductive paths (Johnson and Graham, 1993). As a result, high frequency currents tend to concentrate near the surface of the conductor due to internal inductance which subsequently minimizes the effective cross-section area of the trace. Subsequently, this will result with increasing high frequency resistance following the Equation 2.18.

Next, skin depth (δ) is defined as the depth at which the wave is exponentially attenuated to e^{-1} or 37% of the surface wave intensity (where a constant e=2.718). For conductor, the skin effect (δ) depth of the penetration is estimated by Equation 2.19 (Cheng, 1989):

$$\delta = \frac{1}{\sqrt{\pi f \mu \sigma}} \quad \text{(m)} \tag{2.19}$$

where, f is the frequency, μ is the material permeability and σ is the conductor conductivity. For general non-magnetic materials such as copper, the permeability is assumed equal to be a unity (i.e. 1).

Figure 2.3 shows skin depth plots of two common conductors; copper (σ=5.7x10^7 S/m) and aluminum (σ=3.7x10^7 S/m) versus frequency. Evidently, the higher conductivity material (i.e. copper) experiences a lower skin depth at lower frequency (i.e., $\delta \alpha \frac{1}{\sqrt{\sigma}}$ from Equation 2.19). This also indicates that higher conductivity materials are more effective for electromagnetic (EM) wave shielding by providing lower EM waves penetrations.

Figure 2.3 also unveils significant information linked to conductor loss analysis. Skin effect loss is insignificant for thin conductors less than 1μm such as the one used on MMICs or silicon interconnects up to 10 GHz since the skin depth is already much larger than the conductor thickness, hence, can be assumed similar the DC resistance (Braunisch and Grabinski, 1998). However, for PCB with typical conductor thicknesses of 25μm to 50μm the same conclusion is unfounded since the conductor thickness is bigger than skin effect depth. Clearly from Figure 2.3, PCB skin effect losses are significant even at low frequency operations (<10Ghz). This is the key difference

between MMIC and PCB to be highlighted in this section in relation to the skin effect impact to high frequency signals.

After introducing the skin effect theory, Equation 2.18 can now be rewritten to include frequency dependent skin depth effect as the following:

$$R_{ac} = \frac{\rho}{A_{eff}} \qquad \text{(ohm/m)} \qquad (2.20)$$

where, A_{eff} is the frequency dependent effective cross-section area.

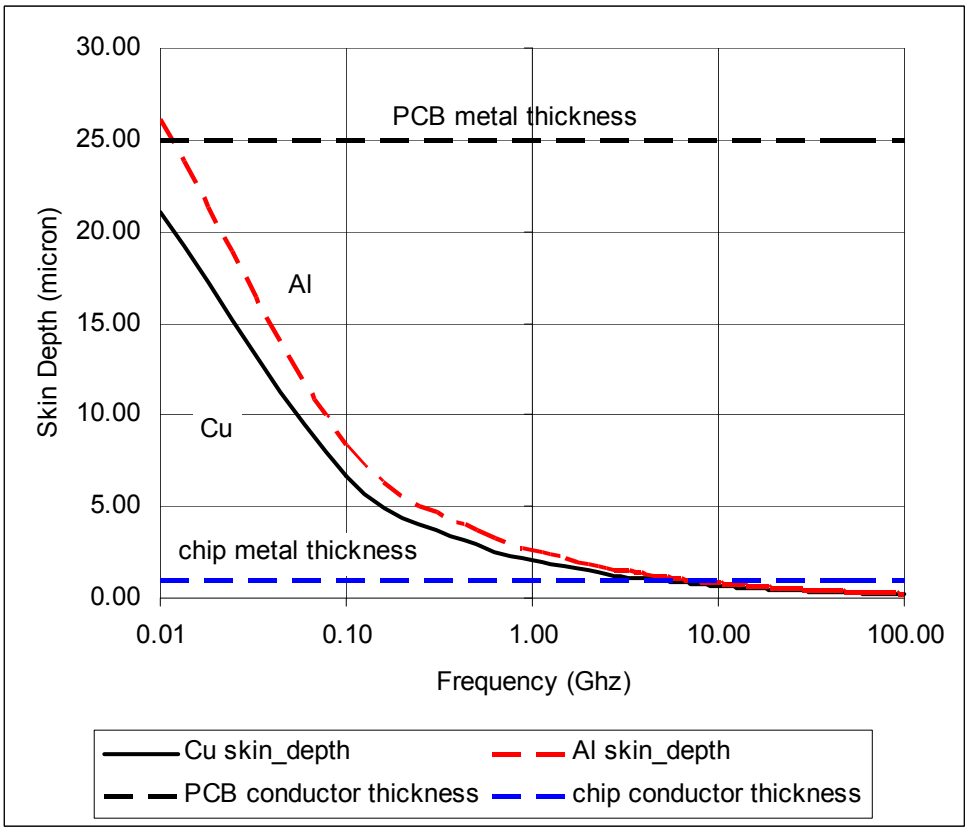

Figure 2.3: Skin depths of two different conductors (copper and aluminum).

In general, the effective cross-section area (A_{eff}) estimation is nontrivial since depending heavily on the electromagnetic (EM) field patterns that are also dependent on transmission line geometry and dimension. Microstrip's current density distribution estimates, i(x) under the signal line is given below (Pucel et al., 1968; Johnson and Graham, 1993).

$$i(x) = \frac{I_o}{\pi h}\left[\frac{1}{1+(x/h)^2}\right] \qquad \text{(A)} \qquad (2.21)$$

where, I_o is the current magnitude, h is the dielectric height and x is distance away from the center of the signal trace. Figure 2.4 below illustrates the current distributions as plotted using Equation 2.21 that show the current density is gradually diminished when moving away from center of the conductor strip.

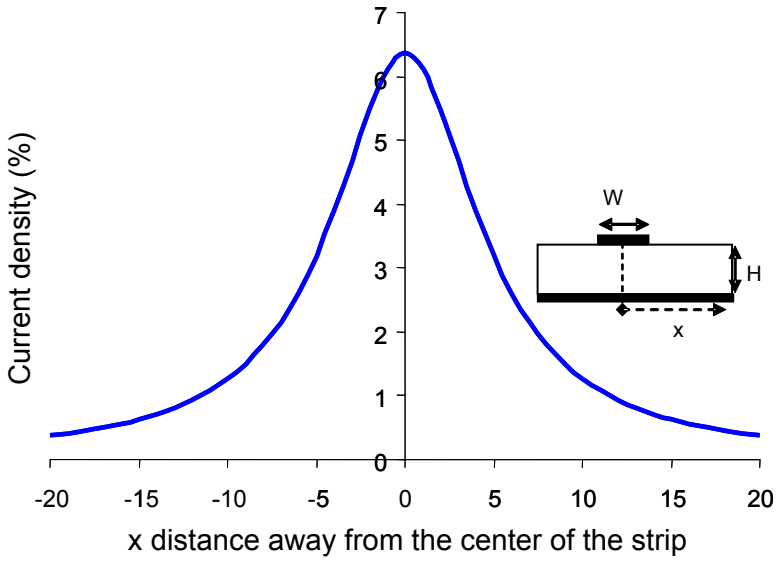

Figure 2.4: Reference plane current density estimation underneath a microstrip trace (in percentage of I_o) using Equation 2.21 for h=127μm, w=200μm and I_o=1A.

Equation 2.21 and Figure 2.4 show that current distributions under a signal trace can be confined tightly beneath the trace by utilizing a thinner dielectric height (h). Crosstalk to adjacent circuits can be avoided by confining return current closer below the trace to avoid interfering with currents from neighboring circuits. Therefore, one of the effective and cheap methods to avoid crosstalk is to apply thinner dielectric materials whenever feasible in order to minimize crosstalk.

Fortunately, most of today's field solvers such as from CST, Agilent and Ansoft are capable simulating current density effect accurately and timely as shown in Figure 2.5 below that is produced using a software from Ansoft Corporation called 2D

Extractor™. Figure 2.5 illustrates the currents disperse into a bell-like curve in a similar fashion as predicted by Equation 2.21 and Figure 2.4.

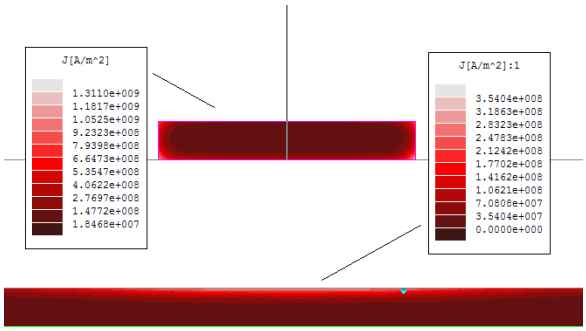

Figure 2.5: Microstrip current distribution at 100 MHz (current density Amp/m^2 for trace and reference plane conductors). Channel details: ε_r = 3.9, trace width, w = 254μm and trace thickness, h = 36μm.

Next, Figure 2.6 illustrates 2D Extractor™ plots of the current distributions on a microstrip line at different frequency intervals; 10Hz, 1 MHz, 100 MHz and 1 GHz. At lower frequency (10MHz), currents are uniformly distributed across the strip in as similar fashion as the DC case. However, higher frequency currents are concentrated beneath the conductor surface. Figure 2.5 and Figure 2.6 offered powerful visual proofs regarding frequency dependent resistance concepts brought forward in this section.

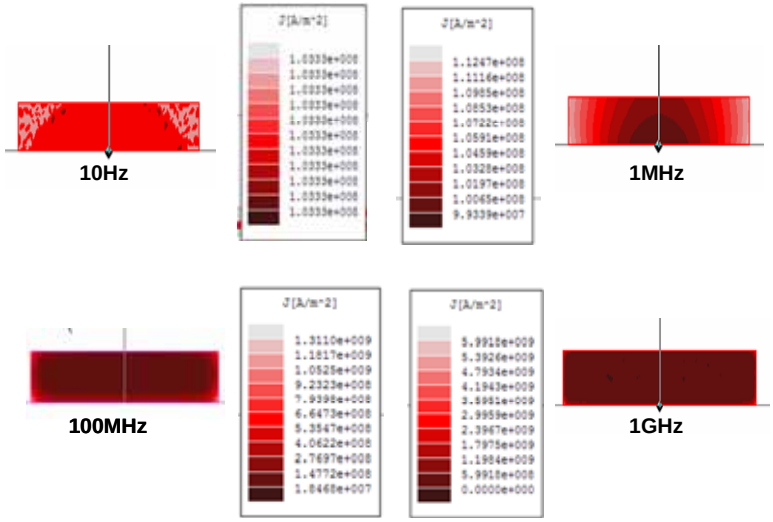

Figure 2.6: Current distribution on microstrip trace at various frequency points. Darkest regions indicate lowest current density for each plot (bottom reference ground current density distribution is omitted for brevity).

2.4 Review of Planar Transmission Line Structures

Since this thesis discusses about signal propagation on a planar transmission line, this section gives a quick preview of most common planar transmission lines as illustrated in Figure 2.7. Microstrip (MS) is probably the most popular transmission line of choice for MMIC, IC and PCB (Figure 2.7a). MS is formed by a conductor strip on a dielectric insulator with a conductor plane at the bottom and typically air at the top (Ramo et al., 1993; Pozar, 1998). MS cannot support a true TEM wave propagation since the dielectric materials surrounding the strip are inhomogeneous. The main driver for microstrip popularity is credited to simpler fabrication process using conventional processes. The disadvantages of microstrip are pointed to the requirement for a minimum of two metal layer and vertical vias interconnects and vulnerable to dispersion and radiation at high frequency region.

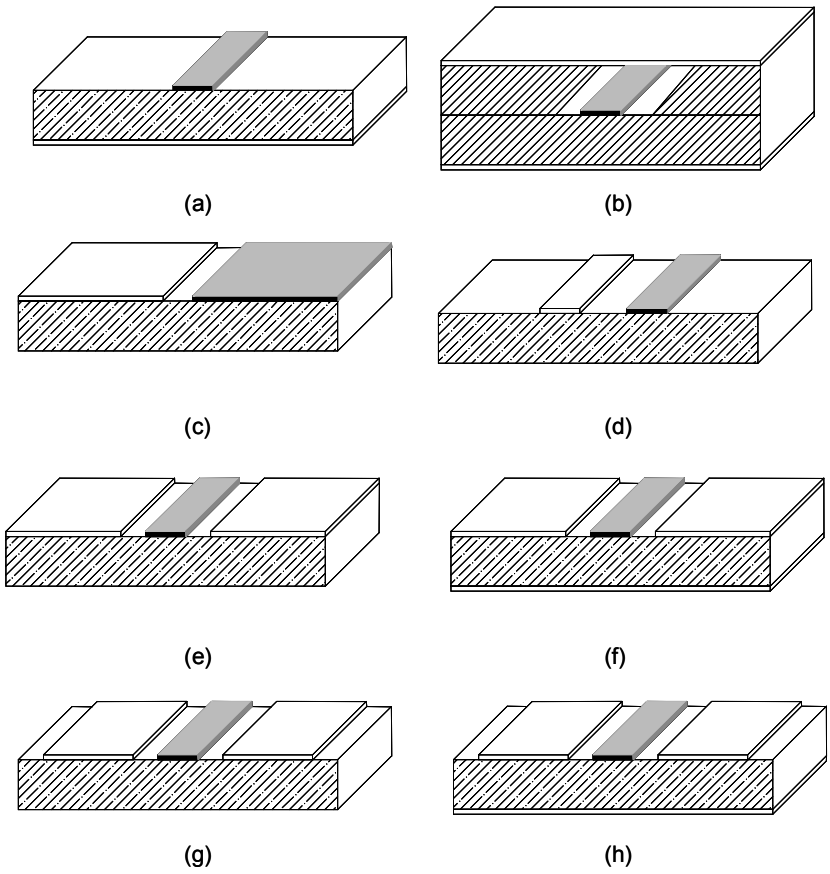

Figure 2.7: Common planar transmission lines (a) microstrip line (b) stripline (c) slot-line (d) co-planar stripline (e) conventional coplanar waveguide (f) conductor backed coplanar waveguide (g) finite width coplanar waveguide, and (f) finite width conductor backed coplanar waveguide.

Stripline (Figure 2.7b) is another popular transmission line formed by embedding a strip between two conducting planes that are separated by dielectric materials (typically of the same material). Since the material is homogenous, stripline is non-dispersive and capable to support TEM wave propagation (Cohn, 1954, Ramo et al., 1993; Pozar, 1998). One big advantage of stripline is on excellent immunity to crosstalk and emissions providing by the adjacent planes. Stripline is highly scaleable that make it a natural preference for multilayer interconnects for backplanes and device packaging substrates. Stripline disadvantages are pointed to its construction that requires multiple conductor layers for signal and power sources along with the associated conducting vias to tie them together.

Slotline (SL) was originally introduced by Cohn in 1968 as an alternative to microstrip line (Figure 2.7c) (Cohn, 1968; Mariani, 1969). SL consists of two strips on the same layer of dielectric material that is separated by a slot. Similar to MS, true TEM wave propagation is not supported by SL due to inhomogeneous dielectric mediums. Even though slot line is popular on MMIC, it is rarely being implemented on PCB because of its strips tend to radiate even at low frequency (i.e. behaving similar to patch antenna).

Coplanar stripline (CPS) is another example of two-conductor transmission line similar to MS and SL (Figure 2.7d) (Ramo et al., 1993). CPS does not support true TEM mode of propagation as well due to inhomogeneous dielectric materials. Its uni-planar design is very versatile and easy to implement on MMIC processes. CPS has been demonstrated to provide excellent signal propagation for very fast pulses (Frankel et al., 1992). Unlike SL, CPS strip widths can be adjusted to control radiation and resonance without the need for costly suppression solutions such as stitching vias or

air bridges. However, due to lack of shielding, CPS is susceptible to high frequency crosstalk from neighboring circuits (Goverdhanam et al., 1997).

Coplanar waveguide (CPW) was originally proposed by C. P. Wen from RCA Laboratory in 1969 (Figure 2.7e). The original design assumed the adjacent ground strip widths and dielectric thickness were infinite. Over the years, many inventors modified the design to achieve superior attenuation and dispersion characteristics for meeting specific applications. Some designs are revolutionary such as by using an elevated center strip or by adding air groove underneath the signal strip (Jeong et al., 2001; Wu, Xu and Bosisio, 1994) in order to minimize dielectric interface discontinuities (i.e. dispersion). However, mostly of these recommendations are specific MMIC applications and not many finds their ways into mainstream PCB implementations.

2.5 CPW Literature Review

This section covers the literature reviews related to CPW covering its applications, propagation characteristics and issues in order for us to narrow down a CPW variant that is suitable for PCB applications. Figure 2.8 depicts the conventional CPW envisioned by Wen in 1969. Since CPW inception, MMIC's CPW interconnects were reported to operate up to 100GHz more than a decade ago (Riaziat, 1989). Lately, CPW is no longer exclusively for MMIC, but also has found its application onto high frequency 50GHz silicon interconnects as well (Kleveland et al., 1998). In addition, CPW structures were also reported to be used for off-chip interconnects such as on high performance flip-chip assembly packaging for MMIC (Wen et al.,1995; Pillai, 2002; Hirose et al., 1998) and high performance test fixtures (Gronau and Felder, 1993). Other applications using CPW structures are micro-electromechanical systems (MEMS) based switches, phase shifters, filters, printed circuit antenna (Simons, 2001) sensor (Khalid and Hua, 1998) and characterization jigs for material measurements (Mbairi and Hesselbom, 1998).

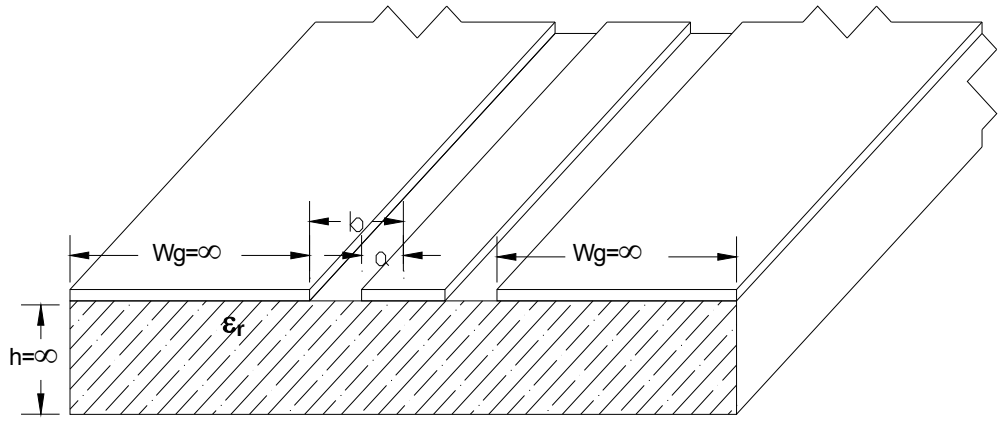

Figure 2.8: A perspective view of a conventional coplanar waveguide (CPW) showing signal trace width (w) of 2a, and air gap distance of (b-a). Side strip widths and dielectric material thickness are assumed extending to infinity.

However, since this work is intended for a larger scale PCB implementation, a configuration as shown in Figure 2.9 below is proposed to provide mechanical robustness, power delivery efficiency and natural thermal dissipations paths to the reference planes for the active components. This CPW variant is commonly referred as conductor-backed CPW (CB-CPW).

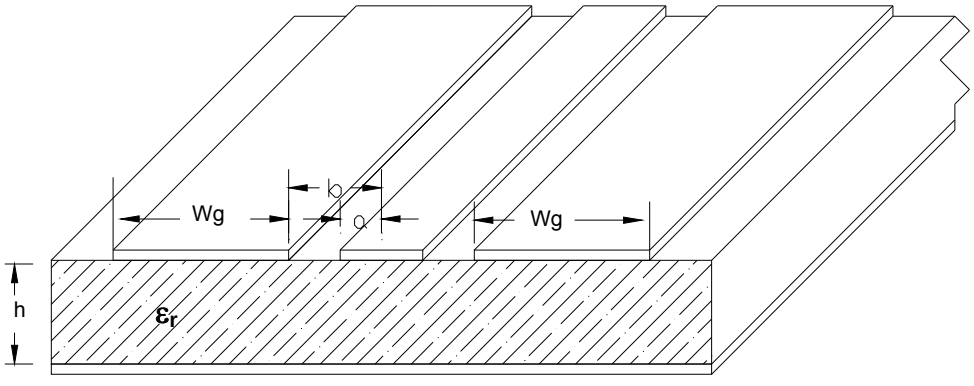

Figure 2.9: A perspective view of CB-CPW showing the critical parameters. Side strip widths (W_g) are assumed extending to infinity for mathematical calculations, signal trace width (2a), air gap (b-a), dielectric thickness (h), and dielectric constant (ε_r).

2.6 CPW Attributes

There many advantages of CPW circuits cited by various sources where some of the significant ones are listed below.

2.6.1 CPW Advantages

i) Immediate access to adjacent power planes provides shorter power delivery path (i.e. lower inductance) to boost active devices performance (Wolf, 1993).

ii) Bottom reference plane provides structural strength (Simon, 2001).

iii) In some cases, CPW gives lower conductor losses and dispersion (Wolf, 1993; Schlechtweg et al.,1994; Jackson, 1986, Shih, 1991)

iv) CPW enjoys smaller radiation at discontinuities as a result of no connecting via (El-Badawy and El-Sharawy, 1992; Jackson, 1989; Görur and Karpuz, 2000)

v) Adjacent strips provide excellent isolations to minimize crosstalk on the same metallization layer (El-Badawy and El-Sharawy, 1992)

vi) Lower crosstalk improves MMIC layout density between 30% to 50% compared to microstrip (Wolf, 1993; Grönau and Felder, 1993)

vii) Planes provide masses for natural thermal cooling thus avoiding the need for external heat sinks for active devices (Simon, 2001).

viii) CPW is 30% cheaper on MMIC fabrication that is contributed by simpler processing steps (Ponchak et al., 1998)

ix) CB-CPW provides lower impedance transmission lines (Simon, 2001).

2.6.2 CPW Disadvantages

Likewise, there are also disadvantages of CPW circuits where some are listed below.

i) Parallel plate configuration produces zero cutoff frequency mode (Wolf, 1993; Magerko, Fan and Chang, 1992)

ii) CPW without conducting plane has lower thermal dissipation and lower structural strength (Simon, 2001).

iii) In general, CPW experience higher losses compared to microstrip (Wolf, 1993).

iv) High frequency losses due to over-moding are more prevailing on CPW than microstrip (El-Badawy and El-Sharawy, 1992).

v) CPW side strips generate both odd and even modes current that can cause serious mode coupling (Ponchak, Papapolymerou and Tentzeris, 2005).

2.7 Review of CB-CPW Design Parameters

Unlike microstrip, CPW has more design parameters that need tweaking in order to obtain the desired dispersion and attenuation performances. It has been shown that a conventional MMIC CPW has a better or equal performance compared to microstrip line depending on the structure designs (Jackson, 1986). However, there are many issues related to CB-CPW such as surface wave leakages, unexpected crosstalk, significant distortion to the guided wavelength (i.e. dispersion), and radiation (Shigesawa and Tsuji, 1988).

In addition to these issues, Gopinath (1979) had shown that when the dielectric height of the CPW equals to the ground plane spacing, conductor and dielectric losses are lowered on microstrip line. For these reasons, CB-CPW design warrants thorough analyses of all parameters to guarantee proper circuit functionality as well as performance; otherwise, it can be just comparable or worse than microstrip line (El-Badawy et al., 1992; Shigesawa et al., 1988). In other words, blind duplication of MMIC rules for PCB design can potentially cause catastrophic failure to circuit operations. These concerns will be answered in this dissertation.

CHAPTER 3

RESEARCH METHODOLOGY

3.0 Introduction

This chapter will highlight methodologies that will be employed in this thesis covering all the three major areas namely frequency and time domains analyses as well as measurements.

3.1 Frequency Domain Analyses

3.1.1 Numerical Frequency Domain Analysis Approach

Closed loop CB-CPW QS-TEM design equations will be derived using the available references from Ghione and Naldi (1987) and Simon (2001). Then, the transmission line propagation constants will be added into the QS-TEM for frequency domain numerical analyses for design optimizations. These processes are illustrated in Figure 3.1.

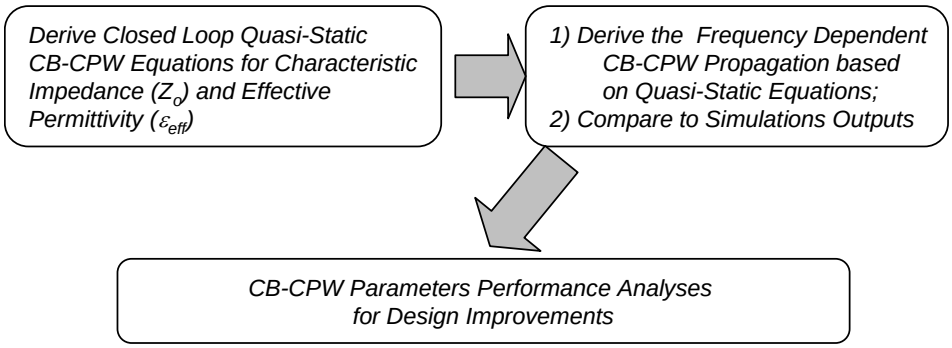

Figure 3.1: Frequency Dependent Equations Development Flows and Performance Analysis.